2025 IEEE/SICE International Symposium on System Integration (SII)
January 21-24, 2025, Munich, Germany

Multi-fingered Robotic Hand with Shape Flexibility for Expanding the Feasible Range of In-hand Manipulation

Masato Morita, Hikaru Arita, Ayato Kanada and Kenji Tahara

***Abstract*— In-hand manipulation with multi-fingered robotic hands is often limited by the restricted range of finger postures that can be achieved when handling objects. Expanding this range is crucial for enhancing the dexterity and versatility of robotic hands in various applications, such as assembly and precision tasks. One of the main limitations comes from the structural design of the fingers, which are typically composed of linked mechanisms comprising fixed-length links and rotational joints. To address this issue, this paper proposes the use of continuum robots for the fingers of multi-fingered hands. We detail the design of the robotic hand and its kinematic model using a constant curvature model, followed by simulations of finger reach and actual grasping experiments. The results of the grasping experiment show that the proposed robotic hand significantly expands the graspable range compared to conventional two-link robotic hands, due to its ability to greatly extend, retract, and bend.**

***Index Terms*— Multi-fingered robotic hand, Grasping, In-hand manipulation, Continuum robot.**

I. Introduction

In the industrial field, the use of robots for automation is advancing, with the objective of enhancing the speed and efficiency of production processes for automobiles and home appliances. Grippers that are active in these production lines have been designed to grip specific workpieces, and they are capable of performing specific tasks with great accuracy on repeated occasions. However, conventional grippers are not well suited to performing tasks other than pick-and-place. For example, in situations that require handling a variety of workpieces with different shapes, such as multi-product production or packaging at logistics facilities, conventional grippers are not adequate. In such environments, versatility can be achieved through regrasping, whereby the workpiece is regripped in order to change its position and orientation, or by replacing the gripper [1]. However, regrasping or replacing the gripper not only takes time, which reduces work efficiency, but also carries the risk of dropping the workpiece. In addition, there may be cases where these operations cannot be performed due to workspace constraints. In these cases, in-hand manipulation with a multi-finger robotic hand, where the position and orientation of the object can be fully controlled within the hand, is effective [2], [3]. Despite the advantages, the range of position and orientation control of objects through in-hand manipulation is constrained by the limitations of conventional multi-finger robot hands. Most multi-finger robot hands use fixed-length links and rotational joints. For example, when manipulating an object as shown in Fig. 1, bending a finger as in Fig. 1(a) results in interference between the links, preventing further bending. Moreover, the rotational joints between the links protrude, which may result in contact with the surrounding environment. These physical interferences limit the possible positions and orientations of the fingertips. Furthermore, during in-hand manipulation, multiple fingers must maintain contact with the workpiece to prevent it from falling, which indirectly constrains the movement of the fingers relative to one another. This constraint further limits the reachable positions and orientations of the fingertips. As a result, the range of positions and orientations of the grasped object is significantly reduced due to mechanical interference inherent in common link structures.

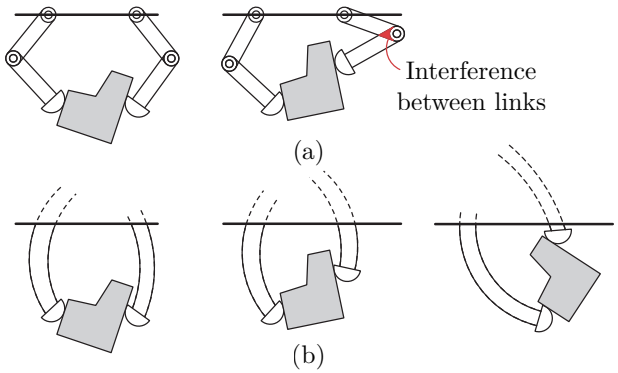

Fig. 1. The hand with continuum fingers can reach a wider range of motion compared to conventional hands, which are limited in motion by interference between the links. (a) Two-finger robotic hand with conventional rigid links. (b) Continuum robot for fingers.

In this study, we consider relaxing the constraints of fixed link lengths and rotational movement only at the joints. As shown in Fig. 1(b), if the finger itself can vary in length and the entire finger can deform, the range of motion of the finger expands. The reachability of the fingertips expands, allowing a wider range of contact points with the object and enabling grips that are difficult to achieve with conventional link structures. We define this characteristic as "shape flexibility," which refers to the ability of the entire robot to deform by extending and bending. With shape flexibility, multiple gripping strategies can be employed, enabling extensive in-hand manipulation.

*This work was partially supported by JSPS KAKENHI Grant Number JP24H00726.

The authors are with Department of Mechanial Engineering, Kyushu University, Fukuoka 819-0395. JAPAN (e-mail: morita@hcr.mech.kyushu-u.ac.jp; arita@ieee.org; kanada@mech.kyushu-u.ac.jp; tahara@ieee.org)

As a structure with shape flexibility, continuum robots inspired by the flexible structures of biological organisms such as elephant trunks and octopus arms have been proposed [4], [5]. Continuum robots are not constrained by rigid link structures and have a wide range of motion in their shape. In particular, Parallel-continuum robots (PCR) have been proposed as structures that can achieve both significant extension and bending movements [6]. PCR consist of multiple elastic rods arranged in parallel, allowing for potential deformations through both extension and bending. However, rods without length constraints can produce significant extension but lack structural rigidity and shape constraints between the rods, making them unsuitable for tasks that require grasping or transporting objects. Matsuda et al. [7] addressed this issue by proposing a robotic arm that combines high rigidity and a wide range of reachable positions using flexible rack gears and rigid link chains instead of elastic rods. By rotating the gears attached to the motors, the rack gears move, allowing for extension when the motors on both sides rotate at the same speed and bending when they rotate at different speeds. If the mechanism proposed in [7] with these characteristics can be adapted for fingers, it is expected to achieve extensive in-hand manipulation due to the wide range of fingertip reach mentioned earlier.

However, there are significant differences in design specifications, including size, between robotic arms and robotic fingers, making it difficult to directly apply the design proposed in [7] to robotic fingers. Additionally, while the robotic arm proposed in [7] is mainly intended for use as a single unit, in-hand manipulation with robotic fingers is primarily performed through the coordination of multiple fingers. Therefore, this study aims to develop robotic fingers that can take a wide range of fingertip positions and orientations by adapting the design in [7] while considering these differences.

Manipulation with continuum robots has primarily been conducted through power grasping [8], [9]. However, precision grasping, which involves pinching objects with the fingertips, is better suited for more dexterous manipulation, as it involves fewer constraints at the contact points [3]. Thus, this study focuses on precision grasping.

In the following sections, after discussing the design of the robotic fingers, we will conduct simulations of the grasping range and perform grasping experiments with the actual device to demonstrate the effectiveness of the proposed method in achieving a wider range of in-hand manipulation using the continuum fingers.

II. Robot Design

This chapter presents the design and structure of our robotic finger, which has developed based on the robotic arm proposed in [7]. The details of this design are discussed in [10]. Figure 2 shows the developed robotic finger. Key features and differences from the original robotic arm [7] include:

- Size: While the robotic arm in [7] has a length of approximately 400 mm and a diameter of about 30 mm, our design achieves an effective length of about 100 mm and a diameter under 20 mm. This significant reduction in size allows for use as a finger in a robotic hand.
- Degrees of Freedom: Our finger has 2 degrees of freedom, compared to the 4 degrees of freedom in the original arm. This reduction is offset by the multi-finger design of our robotic hand, allowing for complex manipulations through finger cooperation.
- Manufacturing Approach: To address miniaturization challenges, we used high-precision techniques. The links were produced with a stereolithography 3D printer (Form3, Formlabs), minimizing friction effects that become more prominent at smaller scales.
- Rack Gear: We employed a standard DURACON rack gear (DR0.8-2000, KHK) with a module 0.8 reference rack tooth profile (JIS B1701-1).

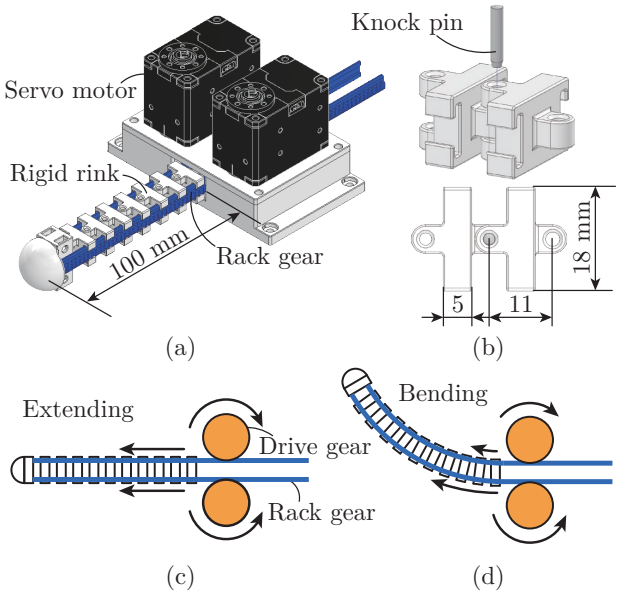

Fig. 2. Schematic diagram of the proposed robotic finger. (a) Overview. (b) Backbone. (c) The robot extends when the drive gears rotate at the same speed. (d) The robot bends when the drive gears rotate at different speeds.

As illustrated in Fig. 2, a 2 mm diameter knock pin is used as a rotational joint. Guides on both sides of the link allow passage for two rack gears. The driving unit comprises servo motors (Dynamixel XL330-M288-T, ROBOTIS) and gears to transmit the motor rotation to the rack gears.

III. Kinematic Model

In this section, we derive the kinematic model of the proposed robot. The forward kinematics is derived to examine the range of positions the fingertip can reach within the operational range of the actual device when the length of the rack is varied. Additionally, the inverse kinematics is derived to perform position control-based in-hand manipulation using two fingers.

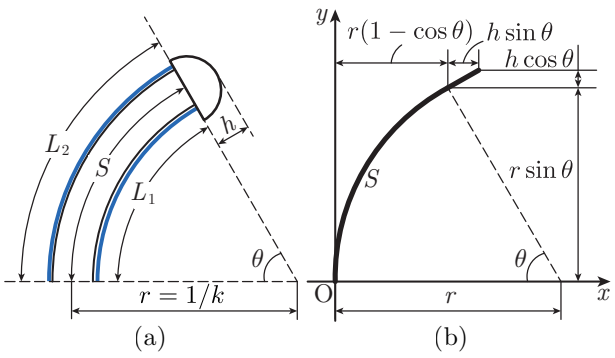

Fig. 3. Top view of proposed robot finger. (a) Definition of the constants. (b) Kinematic model of the robot finger.

A. Forward Kinematics

The robot changes the length of the rack gears by rotating two gears connected to the motors. The fingertip position $\boldsymbol{p} = [x, y]^\top$ is defined by the mapping $f\colon \boldsymbol{L} \to \boldsymbol{p}$, where the length of the rack gears $\boldsymbol{L} = [L_1, L_2]^\top$ serves as the variable. Assuming a constant curvature model [7], [11], [12] commonly used for continuum robots, it is hypothesized that the backbone and the rack gears deform into an arc while maintaining a constant curvature. Based on Fig. 3, $\boldsymbol{L}$ can be expressed using the radius of curvature r and the degree of curvature θ as follows:

$$\boldsymbol{L} = \begin{bmatrix} L_1 \\ L_2 \end{bmatrix} = \begin{bmatrix} \left(r - \dfrac{w}{2}\right)\theta \\ \left(r + \dfrac{w}{2}\right)\theta \end{bmatrix}. \tag{1}$$

Here, w represents the distance between the left and right rack gears. By adding and subtracting the components of (1), $\boldsymbol{q} = [r, \theta]^\top$ is expressed as a mapping $g\colon \boldsymbol{L} \to \boldsymbol{q}$:

$$\boldsymbol{q} = \begin{bmatrix} r \\ \theta \end{bmatrix} = \begin{bmatrix} \dfrac{L_2 + L_1}{L_2 - L_1}\dfrac{w}{2} \\ \dfrac{1}{w}(L_2 - L_1) \end{bmatrix}. \tag{2}$$

Based on Fig. 3, the fingertip position $\boldsymbol{p} = [x, y]^\top$ can be expressed using $\boldsymbol{q}$ with the mapping $u\colon \boldsymbol{q} \to \boldsymbol{p}$ as in (3):

$$\boldsymbol{p} = \begin{bmatrix} x \\ y \end{bmatrix} = \begin{bmatrix} r(1-\cos\theta) + h\sin\theta \\ r\sin\theta + h\cos\theta \end{bmatrix}. \tag{3}$$

Here, h represents the length from the end of the rack gear to the fingertip, as shown in Fig. 3(a). Thus, the forward kinematic model can be expressed as the composite mapping:

$$f = (u \circ g)\colon \boldsymbol{L} \to \boldsymbol{p}. \tag{4}$$

It should be noted that there is an error in the actual curvature of the robot, k. Since this error depends on the desired curvature k_d of the robot, we introduce the error term ε and express it as follows:

$$k = k_\mathrm{d}(1 + \varepsilon). \tag{5}$$

Algorithm 1 Levenberg-Marquardt Algorithm

1: $k \leftarrow 0$
2: $\boldsymbol{e}(\boldsymbol{q_k}) = \boldsymbol{p_d} - \boldsymbol{p}(\boldsymbol{q_k})$
3: **if** $\|\boldsymbol{e}(\boldsymbol{q_k})\| < \delta$ **or** $k > m$ **then**
4: **return** $q \leftarrow q_k$
5: **end if**
6: $\Delta\boldsymbol{q_k} = [\boldsymbol{J}^\top\boldsymbol{W}\boldsymbol{J} + \lambda\boldsymbol{I}]^{-1}\boldsymbol{J}^\top\boldsymbol{W}\boldsymbol{e}(\boldsymbol{q_k})$
7: $\boldsymbol{q_{k+1}} = \boldsymbol{q_k} + \Delta\boldsymbol{q_k}$
8: $k \leftarrow k + 1$
9: **Go to** 2

B. Inverse Kinematics

The inverse kinematics is derived using the relation $f^{-1} = g^{-1} \circ u^{-1}$. While u^{-1} can be easily obtained using (1), deriving g^{-1} analytically is challenging due to the existence of singularities. Although there are methods to avoid singularities by mapping to a different state space than that of $\boldsymbol{q}$ [12], [13], this study uses the Levenberg-Marquardt (LM) method [14], which can robustly compute around singularities, to numerically obtain u^{-1} and solve the inverse kinematics. The Jacobian matrix $\boldsymbol{J}$ is expressed as in (6):

$$\boldsymbol{J} = \frac{\partial u}{\partial \boldsymbol{q}}. \tag{6}$$

When the target position of the fingertip $\boldsymbol{p_d}$ is given, the inverse kinematics calculations were performed using the LM method. The framework is shown in Algorithm 1. The weight matrix $\boldsymbol{W}$ is defined as follows:

$$\boldsymbol{W} = \mathrm{diag}\left(1, \frac{1}{2\pi}\right). \tag{7}$$

IV. Simulation

A. Condition of the Robot

The robot handled in this study can change the lengths of the two rack gears $\boldsymbol{L}$ while satisfying the following two constraints. Here, L_max is the maximum length of the rack gear, and k_max is the maximum curvature of the robot.

$$k < k_\mathrm{max},\ 0 \le L_1, L_2 \le L_\mathrm{max} \tag{8}$$

The maximum curvature k_max is restricted by the structure of the robot when not considering the bending of the rack gear. As shown in Fig. 4, the curvature limitations due to the structure of the robot are considered. As shown in Fig. 4(a), the curvature of the robot is maximized when the side of the robot contacts the preceding link. Given the angle $\alpha = \arctan\left(\frac{l}{w}\right)$ and the lengths l and w, we can analyze the curvature. As shown in Fig. 4(c), consider the circle passing through the joints of each link. If the radius of this circle is r, then $\triangle\mathrm{CBD}$ is an isosceles triangle with $\angle\mathrm{BCD} = 2\alpha$. From the law of cosines, the radius r can be determined, and thus the maximum curvature of the robot is given by:

$$k_\mathrm{max} = \frac{1}{r} = \frac{1}{\sqrt{\left(\dfrac{w}{2}\right)^2 + \left(\dfrac{l}{2}\right)^2} + \dfrac{t}{\sqrt{2(1-\cos 2\alpha)}}}. \tag{9}$$

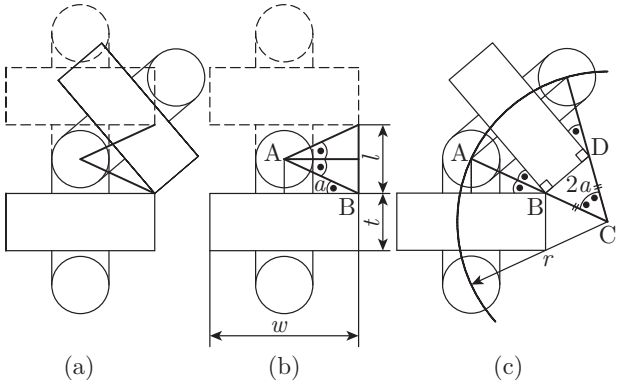

Fig. 4. Curvature limitations due to the structure of the robotic finger. (a) The curvature is maximized when the side of the robot contacts the preceding link. (b) Structural constraints limiting curvature based on link dimensions. (c) Maximum curvature analysis using the circle passing through the joints of each link.

The robot used in this study has $l = 6\,\mathrm{mm}, w = 13\,\mathrm{mm}, t = 5\,\mathrm{mm}$. In this case, $k_{\max} = 0.076\,\mathrm{mm}^{-1}$.

B. Simulation of Reachable Area

The robotic finger proposed in this study is expected to have a wider fingertip reach compared to conventional link-structured robotic fingers. In this section, to clarify the advantages of the proposed robotic finger in terms of fingertip reach, we use the forward kinematics model described in III-A to simulate the fingertip reach of the proposed robotic finger and compare it with that of the link-structured robotic finger. Here, we simulate the fingertip reach when two proposed robotic fingers are placed side by side at a $100\,\mathrm{mm}$ interval and operate as a two-finger hand. The overlapping area of the fingertip reach of the two robotic fingers is considered as the area where sufficiently thin objects can be grasped. Based on the specifications of the prototype, the maximum length of the robot is set to $100\,\mathrm{mm}$ and the maximum curvature to $0.076\,\mathrm{mm}^{-1}$. The link-structured robotic hand is considered as a two-link structure here, with each link length set to $50\,\mathrm{mm}$, and the range of motion of each joint set to 0 to $120°$. The results are shown in Fig. 5 and Fig. 6. The proposed robotic hand has a wider fingertip reach near the origin, resulting in a larger overlapping region of fingertip reach compared to the conventional link-structured robotic hand. Specifically, the overlapping region with the proposed finger is $14.77\,\mathrm{cm}^2$, which is $1377\,\%$ larger than the overlapping region of $1.00\,\mathrm{cm}^2$ achieved when the two-link hand bends by $50°$. Figure 6 illustrates how the reachable area and overlap area for the two-link hand depend on the joint angles. The reachable area is represented by the blue solid line, while the overlap area is shown by the orange solid line. The dashed lines in Fig. 6 represent the area for the situation depicted in Fig. 5(b), which does not depend on the angle. To achieve the same overlapping area with the two-link hand, each joint needs to bend by $99°$. However, as mentioned in the introduction, achieving such a degree of bending in both clockwise and counterclockwise directions is highly challenging due to interference between links and other structural constraints. Therefore, it can be said that the proposed robotic hand has a wider grasping range than the conventional link-structured robotic hand.

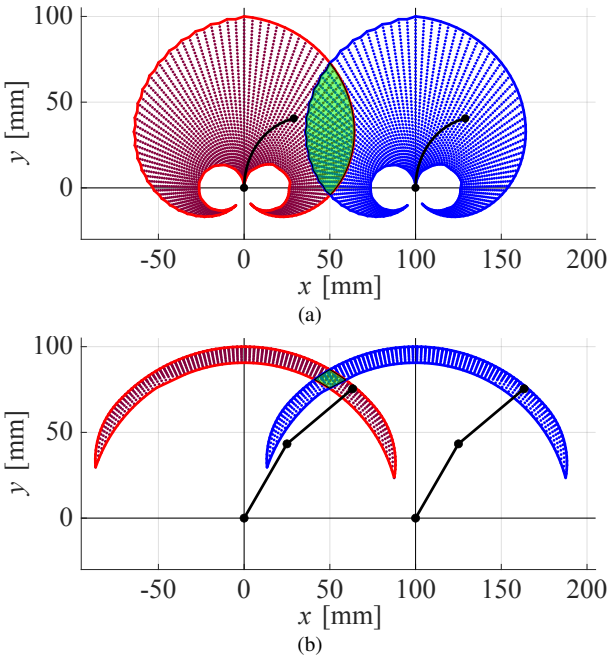

Fig. 5. Finger reach comparison using two finger. The area in red and blue is the reach of one finger and the area in green is the overlapped range of two fingers. (a) Proposed robotic fingers. (b) 2DOFs fingers with restriction angle $50°$.

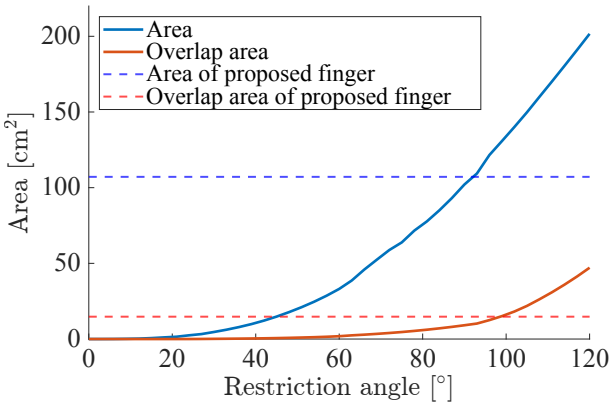

Fig. 6. Comparison of reachable area with restriction angle. The blue solid line represents the reachable area of the 2DOFs fingers shown in Fig. 5(b), while the orange solid line represents the overlap area in the same figure. The dashed lines correspond to the areas in Fig. 5(a), which do not depend on the angle.

C. Comparison of Constant Curvature Model and Actual Device

In (5), it is assumed that the robot's curvature includes an error. In this section, we identify this error and propose a method to correct the robot's curvature. The experimental procedure is outlined. First, the lengths of the left and right rack gears L_1, L_2 are set to $100\,\mathrm{mm}$, and the robot finger is

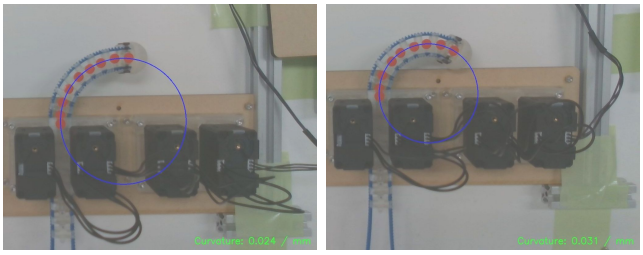

(a) (b)

Fig. 7. Experimental setup for curvature verification. (a) Measurement of curvature before error correction, showing a deviation from the target curvature. (b) Measurement of curvature after error correction, where the actual curvature closely matches the target curvature, as indicated by the alignment of the blue circles representing the estimated curvature.

straightened. At this time, the arc length S of the robot finger is equal to L_1 and L_2. From this straight state, the desired curvature k_d is assigned specific values by adjusting the lengths of the left and right racks, while maintaining the arc length S of the robot finger. The curvature k_d is varied from $0.01\,\mathrm{mm}^{-1}$ to $0.05\,\mathrm{mm}^{-1}$ in increments of $0.01\,\mathrm{mm}^{-1}$, and experiments are conducted within the range where the robot does not interfere with the drive unit. For the experiments, red markers are attached to the robot hand as shown in Fig. 7. One marker is placed on the base of the robot, one near the fingertip, and one on each joint of the link. These markers are captured using a camera (RealSense D435i, Intel). The position of the camera relative to the robot hand is adjusted so that the entire finger fits within the camera's field of view. The camera's resolution is set to 1920×1080, and the camera is fixed at a position where 250 pixels on the camera correspond to $50\,\mathrm{mm}$. The positions of the markers are measured, and a circle is fitted to these positions. The reciprocal of the radius of this circle represents the curvature.

The experimental results are shown in Fig. 8(a). It is found that the longer the arc length S of the robot finger, the closer the measured curvature k gets to the target value. When the arc length of the robot finger is short, the curvature does not reach the target value. This is due to the strong constraint that the robot remains straight at the drive unit near the robot finger base.

The error ε in (5) depends on the arc length S of the robot finger, so we assume that ε is linear with respect to S and express it as follows:

$$\varepsilon = aS + b. \tag{10}$$

Substituting (10) into (5), it can be expressed as follows:

$$\frac{k}{k_\mathrm{d}} - 1 = aS + b. \tag{11}$$

Using (11), linear regression is performed to obtain the correction coefficients a and b. In this experiment, $a = 0.0013, b = -0.2774$. When the operation is corrected using the estimated correction factor, it can be seen that the curvature approaches the target curvature as shown in Fig. 8(b).

V. Grasping Experiment

In the overlapping region of the fingertip reachability discussed in IV-B, we conduct experiments to verify that the robot hand can perform grasping and in-hand manipulation. These experiments include the grasping of a sponge and position-controlled in-hand manipulation based on the inverse kinematics presented in III-B. The results are shown in Fig. 9.

In Fig. 9(b), the robot hand successfully grasps the sponge. To perform in-hand manipulation, the two fingers are coordinated by aligning the target positions of their fingertips. A circular trajectory $(x-50)^2 + (y-70)^2 = 20^2$ is set as the target path in a coordinate system where the origin is at the base of the left finger. This target trajectory is generated using the inverse kinematics derived in III-B, and the corresponding control commands are applied to the servo motors to follow the desired path. As shown in Fig. 9(c) to (f), the robot hand successfully follows the circular path, maintaining the object on the trajectory without dropping it. This manipulation utilizes the wide overlapped range of the two fingers, as shown in Fig. 5(a), which would be difficult to achieve with conventional robotic hands. Figure 9(g) to (l) shows the results of in-hand manipulation where the target trajectory of the fingertip is set to a straight line at $x = 50$ $(20 \leq y \leq 100)$. This in-hand manipulation effectively utilizes the extending and retracting capabilities of the robotic hand, taking full advantage of the wide grasping range illustrated in Fig. 5(a).

It should be noted that the in-hand manipulation demonstrated in this experiment is based on position control, which requires precise pre-planning.

VI. Conclusions

To mitigate the limitations on fingertip reach caused by the link structure and achieve a wide fingertip reach, we proposed applying the robotic arm proposed by [7] as a multi-finger robotic hand. Considering the design constraints for miniaturization, we developed the robotic finger. The forward kinematics simulation confirmed that the proposed robotic hand has a wide grasping area. Additionally, we conducted in-hand manipulation using the actual device based on position control with inverse kinematics, demonstrating that in-hand manipulation utilizing the broad fingertip reach verified in the simulations is feasible. In the future, we plan to equip the device with sensors and pursue research to achieve force-controlled in-hand manipulation.

References

[1] P. Tournassoud, T. Lozano-Pérez, and E. Mazer, "Regrasping," in *Proc. IEEE Int. Conf. Robot. Autom.*, vol. 4, 1987, pp. 1924-1928.

[2] R. Ma and A. Dollar, "Yale OpenHand Project: Optimizing Open-Source Hand Designs for Ease of Fabrication and Adoption," *IEEE Robot. Autom. Mag.*, vol. 24, no. 1, pp. 32 – 40, 2017.

[3] R. Ozawa and K. Tahara, "A Brief Survey on Control of Multi-fingered Robotic hands," *J. Robot. Soc. Jpn.*, vol. 36, no. 5, pp. 306 – 315, 2018.

[4] M. W. Hannan and I. D. Walker, "Kinematics and the Implementation of an Elephant' s Trunk Manipulator and Other Continuum Style Robots," *J. Robot. Syst.*, vol. 20, no. 2, pp. 45 – 63, Feb. 2003.

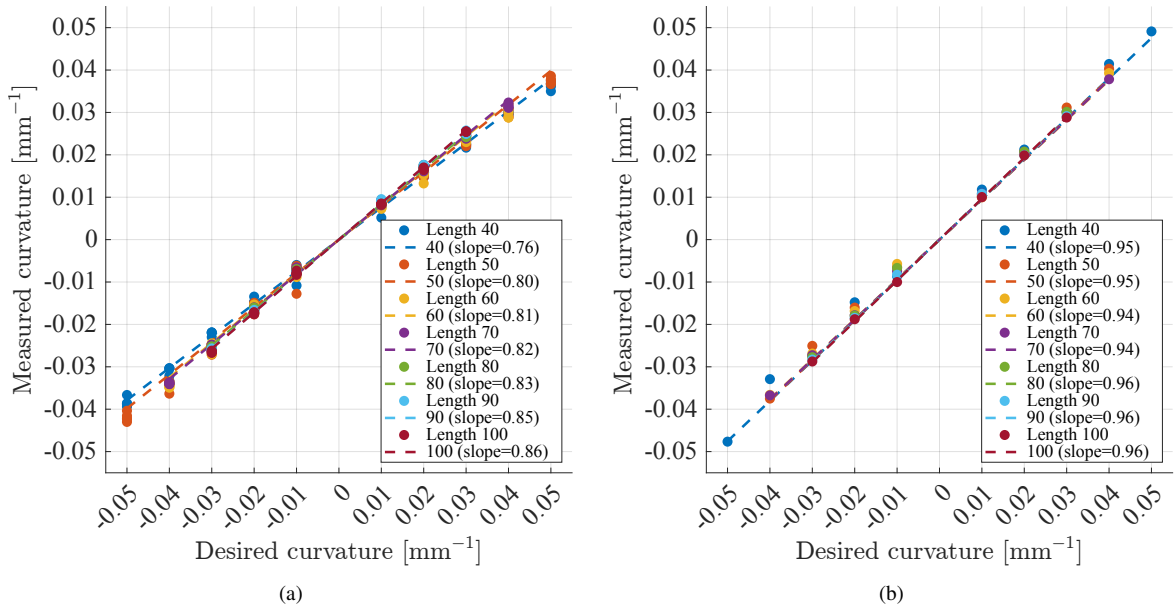

(a) (b)

Fig. 8. Results of the curvature verification experiments. (a) Measured curvature before applying error correction. The curvature deviates from the target as the arc length decreases. (b) Measured curvature after applying error correction. The curvature closely matches the target across all arc lengths.

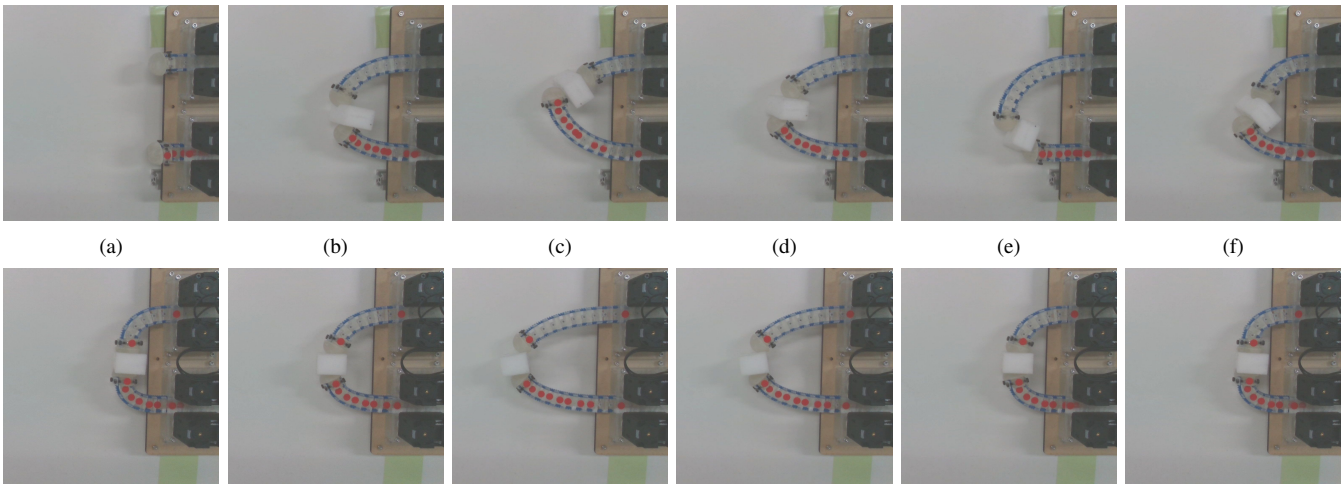

(a) (b) (c) (d) (e) (f)

(g) (h) (i) (j) (k) (l)

Fig. 9. Results of the grasping experiments with the proposed robotic hand. (a)(b) Successful grasping of a sponge. (c)-(f) Snapshots of the in-hand manipulation where the robot hand follows a circular trajectory, maintaining the object securely on the path without dropping it. Snapshots of the in-hand manipulation where the robot hand follows a straight-line trajectory.

[5] P. K. Singh and C. M. Krishna, "Continuum Arm Robotic Manipulator: A Review," *Univers. J. Mech. Eng.*, vol. 2, no. 6, pp. 193 – 198, Jun. 2014.

[6] S. Lilge, K. Nuelle, J. A. Childs, K. Wen, D. C. Rucker and J. Burgner-Kahrs, "Parallel-Continuum Robots: A Survey," *IEEE Trans. Robot.*, vol. 40, pp. 3252-3270, 2024.

[7] R. Matsuda, U. Mavinkurve, A. Kanada, K. Honda, Y. Nakashima, and M. Yamamoto, "A woodpecker' s tongue-inspired, bendable and extendable robot manipulator with structural stiffness," *IEEE Robot. Autom. Lett.*, vol. 7, no. 2, pp. 3334 – 3341, 2022.

[8] Y. Dai, Z. Li, X. Chen, X. Wang, and H. Yuan, "A Novel Space Robot with Triple Cable-Driven Continuum Arms for Space Grasping," *Micromachines*, vol. 14, no. 2, 2023.

[9] J. Zhang et al., "Versatile Like a Seahorse Tail: A Bio-Inspired Programmable Continuum Robot For Conformal Grasping," *Adv. Intell. Syst.*, vol. 4, no. 11, p. 2200263, 2022.

[10] M. Morita, A. Kanada, H. Arita, and K. Tahara, "Development of a Multi-fingered Robotic Hand with Shape Flexibility for Extended Kinematic Range of Motion," in *Proc. JSME Annu. Conf. Robot. Mechatron. Robomec*, 1P2-J08, 2024.

[11] Y. Li, D. H. Myszka, and A. Murray, "The Kinematics of Constant Curvature Continuum Robots Through Three Segments," *IEEE Robot. Autom. Lett.*, vol. 8, no. 11, pp. 7631 – 7638, Jan. 2023.

[12] C. D. Santina, R. K. Katzschmann, A. Biechi, and D. Rus, "Dynamic control of soft robots interacting with the environment," in *Proc. IEEE Int. Conf. Soft Robot.*, 2018, pp. 46-53.

[13] C. Della Santina, A. Bicchi and D. Rus, "On an improved state parametrization for soft robots with piecewise constant curvature and its use in model based control," *IEEE Robot. Autom. Lett.*, vol. 5, no. 2, pp. 1001-1008, Apr. 2020.

[14] T. Sugihara, "Solvability-unconcerned inverse kinematics by the Levenberg-Marquardt method," *IEEE Trans. Robot.*, vol. 27, no. 5, pp. 984-991, 2011.